

## DUAL-BAND HELICAL ANTENNAS FOR NAVIGATION RECEIVERS

Nikolay Mikhailovich Legkiy <sup>1</sup>

<sup>1</sup> Department of Radio Engineering and Telecommunication Systems, MIREA – Russian Technological University, RUSSIA.

### ARTICLE INFO

#### Article history:

Received 18 July 2019  
Received in revised form 06  
January 2020  
Accepted 27 January 2020  
Available online 14 February  
2020

#### Keywords:

Antenna phase center;  
Nested helical antenna;  
Antenna modeling;  
GNSS antenna; Helical  
antenna; Multi-frequency  
antenna.

### ABSTRACT

This paper presents a design of a dual-band helical antenna for tracking navigation signals. There were done several calculations and modeling as well were studied characteristics of a prototype model. Nested helical antennas have the advantage to form independently their radiation patterns and to fit together with their phase centers. This advantage can be used to design the radiators of multi-frequency parabolic reflector antennas with rotating polarization.

**Disciplinary:** Radio-frequency Engineering, Geomatics Engineering, GPS/GLONASS/GNSS Technology.

©2020 INT TRANS J ENG MANAG SCI TECH.

## 1. INTRODUCTION

Quite often, there is a need to receive and/or to transmit a signal within certain frequency ranges using an antenna. Multi-band antennas can operate in two basic ways: 1) Using antenna radiators within a band that covers the desired frequency ranges. 2) Combining into an aperture of the antenna the radiators within different ranges.

In the latter case, placing the radiators next to each other while they will be receiving and/or transmitting a signal will lead to interference between them. Additionally, it will distort directional characteristics, impedance and polarization properties [1-9].

Nested helical antennas have the advantage to form independently their radiation patterns and to fit together with their phase centers. This advantage can be used to design the radiators of multi-frequency parabolic reflector antennas with rotating polarization.

When developing the multi-band helical antenna, there is a need to break the frequency spectrum into parts or to filter the separated frequencies out of it. Where it happens, we use diplexers that cause additional energy loss and functional inconveniences. Besides, there could be a problem to separate close frequencies using diplexers. On top of that, the parameters such as power, the width of radiation

pattern and phase center position of a regular helical antenna are dependent on the frequency.

## 2. METHOD

### 2.1 RESEARCH OBJECTIVE

There is the need to fit together several helical antennas that operate within different ranges, namely, to place them on the same axis “into each other” as shown in Figure 1. This is especially relevant when the helical antennas are used as the radiators of the parabolic reflector antenna or as an element of receiving antenna system and (three- or four-element array) of an angle meter. In addition, that requires to fit together the phase centers of radiators within several frequency ranges.

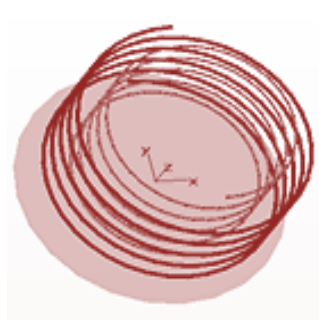


**Figure 1:** Radiator consists of two nested helices

According to [7], a field of the helical antenna can be represented as the sum of the fields of ring radiators with traveling current waves, besides the radiators were placed equidistantly along the z-axis. Then two nested “into each other” helices can be represented as two sets of rings. To evaluate their influence on each other, we need to examine the interaction between two rings that represent different helices and are coplanar. The interaction between rings that are distant from each other along the OZ axis will be weaker because of the bigger distance that is between them than along the OY axis. Thus, we need to consider the model shown in Figure 2. To make it simple, there are a cross-sectional shape of the conductors and square section rings with a side  $2a_3$ . The section of rings in a spherical coordinate system is shown in Figure 3.

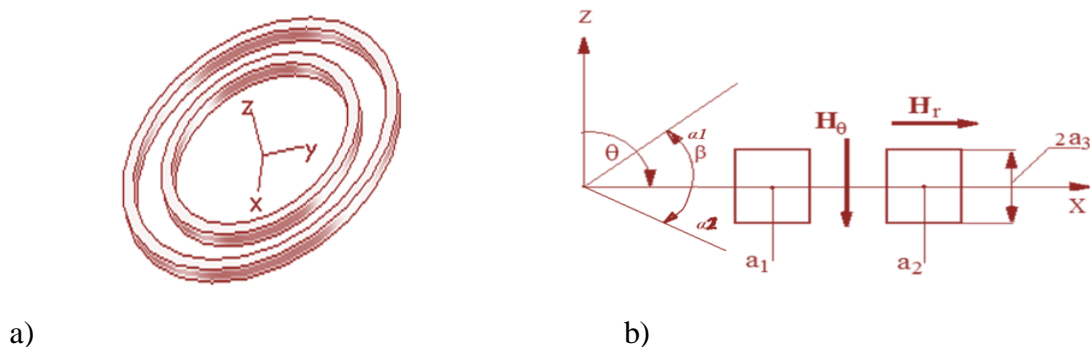


**Figure 2:** Model consists of two rings: a) Model has two rings of square section; b) The section of the model with the two rings is in the spherical coordinate system.

We will believe the first ring with radius  $a_1$  is active, namely, it has an external current, and the second ring with radius  $a_2$  is passive. To estimate the effect of the ring 1 on the ring 2, we need to find the induced current in the ring 2.

The specific nature of this model is that we search for the field in the induction zone, and therefore, the radial coordinate at the observation point  $r$  cannot satisfy inequalities  $r \gg \lambda, a_1, a_2$ ,

where  $\lambda$  is the wavelength. Also, the radii of the rings must be selected according to the working wavelengths of the helices, i.e. based on the ratios:

$$\begin{aligned} 2\pi a_1 &= \lambda_1, \\ 2\pi a_2 &= \lambda_2 \end{aligned} \quad (1).$$

These special aspects do not allow making approximate field calculations using expansion into series per any parameter.

Let's suppose that the current density in the ring 1 is given as the traveling wave:

$$J = J_0 e^{-jkl} \quad (2),$$

where  $J_0$  is the amplitude of the current density,  $l$  is the coordinate of the first ring,

$k = 2\pi / \lambda_l$  is the wavenumber. When counting the azimuthal angle  $\alpha_1$  from the axis OX in the counterclockwise,  $l = a_1 \alpha_1$ .

According to [8], the magnetic vector potential  $A$  will have a single component  $A_\alpha$  that is defined by

$$A_\alpha = \frac{\mu}{4\pi} J_0 \int_V \frac{e^{-jk\rho} e^{-jka_1\alpha_1}}{\rho} dV \quad (3),$$

where  $\mu$  is the magnetic permeability of media,  $V$  is the volume of the ring conductor 1, a  $\rho$  is the distance from the source point to the observation point, and is equal to:

$$\rho = \sqrt{a_1^2 + r^2 - 2 a_1 \cdot r \cdot \cos(\alpha - \alpha_1)} \quad (4),$$

where  $\alpha$  is the azimuthal coordinate of the observation point on the second ring.

Let's assume that the current density on the first ring is spread evenly over its cross-section and taken integral of (3) with respect to this section, we obtain an expression for  $A_\alpha$  as the integral on the azimuthal angle  $\alpha_1$ :

$$A_\alpha = \frac{\mu}{4\pi} I_1 \int_0^{2\pi} \frac{e^{-jk\rho - jka_1\alpha_1}}{\rho a_1} da_1 \quad (5)$$

where  $I_1$  is the amplitude of the total current on the ring.

The magnetic field caused by the current in the ring 1 is determined by the relation  $\mathbf{H} = -1/\mu \text{rot } \mathbf{A}$ , where the operation rot is applied to entering  $\mathbf{A}$  coordinates of the observation point. In the spherical coordinate system, we obtain two components of the magnetic field:

$$H_r = \frac{\cos\theta A_\alpha + \sin\theta \frac{\partial A_\alpha}{\partial \theta}}{\mu r} \quad (6),$$

$$H_\theta = - (A_\alpha/r + \frac{\partial A_\alpha}{\partial r})/\mu \quad (7).$$

The surface current density over the conductor of the second ring is determined by the expression [9]:

$$J_2 = - [n^*H] \quad (8),$$

where  $n$  is the unit vector of the inner normal with reference to the surface of the conductor. If we choose the positive current  $J_2$  flowing in the counterclockwise direction, we get

$$J_2 = H_r(\theta=90^0-\beta, r=a_2) - H_r(\theta=90^0+\beta, r=a_2) \\ - H_\theta(\theta=90^0, r=a_2-a_3) + H_\theta(\theta=90^0, r=a_2+a_3) \quad (9).$$

The total current over the conductor of the second ring will be equal to the product of the surface current density  $J_2$  at the cross-sectional size  $2a_3$ :

$$I_2 = J_2 \cdot 2a_3 \quad (10)$$

Entering (6) and (7), derivatives are determined by

$$\frac{\partial A_\alpha}{\partial \theta} = \frac{\mu}{4\pi} I_0 r \cdot \cos(\theta) a_1^2 \int_0^{2\pi} \frac{\exp(-jk\rho - jka_1\alpha_1)(1+jk\rho + jka_1\alpha_1)}{\rho^3 \cos(\alpha - \alpha_1)} d\alpha_1 \quad (11),$$

$$\frac{\partial A_\alpha}{\partial r} = -\frac{\mu}{4\pi} I_0 a_1 \int_0^{2\pi} \frac{\exp(-jk\rho - jka_1\alpha_1)(1+jk\rho + jka_1\alpha_1)}{\rho^3 r - a_1 \sin(\theta) \cos(\alpha - \alpha_1)} d\alpha_1 \quad (12).$$

Let's substitute (11), (12) and (5) for (6) and (7), and then for (9) and (10), we obtain the expression for amplitude ratio of the total current on the second ring with reference to the current amplitude on the first ring as

$$\frac{I_2}{I_1} = \frac{t^2}{\pi} \int_0^{2\pi} \frac{\exp(-jq - j\alpha_1)}{q(2+p(p+\cos(\alpha - \alpha_1)))} \frac{(1+jq+j\alpha_1)}{q^2} d\alpha_1 \quad (13),$$

where

$$p = a_2/a_1 \quad (14),$$

$$t = a_3/a_2 \quad (15),$$

$$q = \sqrt{1 + p^2 - 2p \cdot \cos(\alpha - \alpha_1)} \quad (16).$$

As well the ratios were considered (1).

As the traveling current wave on the first ring forces up a similar wave on the second ring, it would make sense taking an appropriate exponent out the integral sign in the expression (13).

$$\frac{I_2}{I_1} = \frac{t^2}{\pi} \exp(-j\alpha) \int_0^{2\pi} \frac{\exp(-jq - j\alpha_1 + j\alpha)}{q(2+p(p+\cos(\alpha - \alpha_1)))} \frac{(1+jq+j\alpha_1)}{q^2} d\alpha_1 \quad (17).$$

Using the expression under the integral sign for the azimuth at the observation point  $\alpha$  we can select the real and imaginary parts, calculate the integrals and ultimately determine the module  $|I_2/I_1(\alpha) \exp(j\alpha)|$ .

Calculations show that we can observe a mode of traveling current wave in the second ring that is like the wave in the first ring, but it has the amplitude that depends on the azimuthal coordinate.

The calculation results for the module that indicates this ratio depending upon  $\alpha$  at  $t = 0.01$  for several values  $p = \lambda_2 / \lambda_1 = a_2/a_1$  are illustrated by the graphs shown in Figure 3.

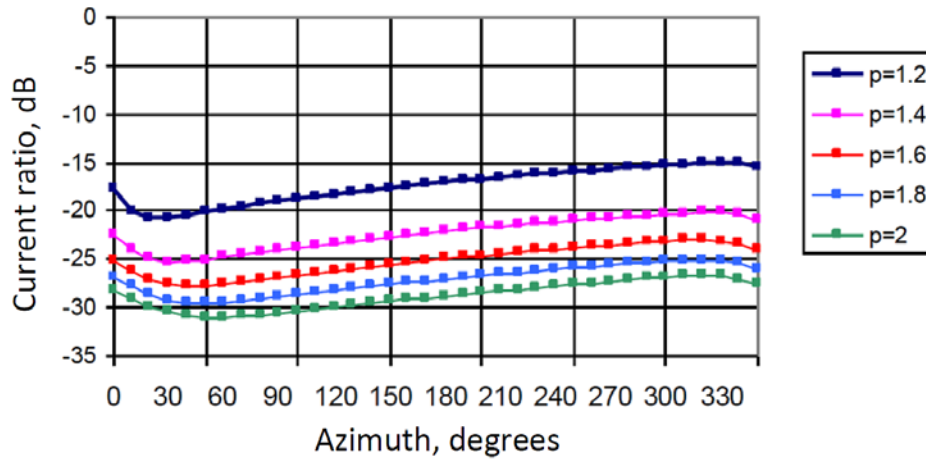


**Figure 3:** The ratio of current in the passive ring with respect to the current in the active one

Obviously, the more operating wavelength of the helices differs, the less current is induced in the passive ring and, accordingly, it has less influence on the radiation pattern of the active helix.

The ratio  $t = 0.01$  means that  $a_3 / \lambda_2 \approx 0.0016$  and, for example, at  $\lambda_2 = 240$  mm,  $a_3 = 0.38$  mm, namely the cross-sectional size of the second ring is equal to 0.76 mm. In addition, the size and ratio of wavelengths  $p \approx 1.2$ , the current amplitude on the second ring does not exceed 3% of the current amplitude on the first ring. In view of  $t < 0.01$  and  $p > 1.2$ , the magnitude of the induced current on the second ring is even smaller.

The induced current on the second ring is proportional to the square of its size  $a_3$  because of two factors: 1) The larger cross-section of the conductor is, the higher the induced current is, according to (10), 2) The currents that are induced on opposite sides of the cross-section of the conductor are contra-directional, in other words, they almost cancel each other out), as the direction of the magnetic field is the same on both sides of the cross-section.

The conducted analysis shows that even though the operating wavelengths of the two nested helices differ by more than 20% and conductor windings are thin the mutual influence of the helices on the radiation patterns is low. This allows creating two or more multi-frequency helical antennas by placing helices on the same axis “into each other”.

## 2.2 CALCULATION OF THE RADIATION PATTERN FOR THE HELICAL ANTENNA

The calculation of the parameters for the helical radiating element (winding parameters), including the right circular polarization with  $FE \approx 1$  is completely presented in [7]. According to the graph [7], we determine the radius of winding  $a$  and the angle of winding  $\alpha$  for wavelength  $\lambda$ . In order to have a single maximum in the radiation pattern, the  $T_1$  wave must be stimulated in the antenna.

The radiation patterns of the monofilar helical antenna are calculated according to the formulas [7]

- in-plane  $\varphi = 0^\circ$ :

$$\begin{aligned} f_\theta &\approx J_0(ka \sin \alpha) \cos \theta \sin(\gamma_0 \pi N) / (\gamma_0^2 - 1), \\ f_\phi &\approx J_0(ka \sin \alpha) \gamma_0 \sin(\gamma_0 \pi N) / (\gamma_0^2 - 1), \end{aligned} \quad (18),$$

where  $N$  is the number of turns,  $J_0$  is the amplitude of the feeding current;

- in-plane  $\varphi = 90^\circ$ :

$$\begin{aligned} f_\theta &\approx J_0(ka \sin \alpha) \gamma_0 \cos \theta \sin(\gamma_0 \pi N) / (\gamma_0^2 - 1), \\ f_\phi &\approx J_0(ka \sin \alpha) \sin(\gamma_0 \pi N) / (\gamma_0^2 - 1), \end{aligned} \quad (19).$$

where  $\gamma_0 = (\beta a - ka \cdot \cos \theta) \cdot \text{tg} \alpha$ .

The radiation pattern of the helical antenna can be approximately considered as a rotation body and use for calculation one of the formulas (18), (19).

## 2.3 EXPERIMENTAL VERIFICATION OF RESULTS

The experimental verification of the calculation results was done during the development of radiators for the reflector antenna — GPS/GLONASS signal receiver module.

To measure the radiation pattern of circularly polarized antennas using a short pulse stroboscopic test unit, similarly, we have designed the antenna that covers the frequency band from 1.1 to 2.3 GHz, shown in Figure 4.



**Figure 4:** The multi-band antenna for the stroboscopic test unit to measure the radiation pattern: a) The antenna with winding for operation with circular polarization; b) A method for tuning the antenna; c) The voltage standing wave ratio (VSWR) for the antenna.

This wideband was achieved by using a matching device, Figure 4a, which provides a smooth transition from a 50 Ohm line to the helical antenna.

When binding a radiator module, we use a low-noise amplifier (LNA), shown in Figure 5, the LNA has a low noise coefficient of about 1.8 dB, has input protection against a constant component and two amplification stages (low-noise transistors with the noise coefficient up to 0.8 dB). Two channels are summed using a summarizer. Power is supplied to the LNA via a high-frequency cable through a voltage stabilizer chip.

Based on this model, there was built the radiator for the reflector antenna in a software environment, shown in Figure 6a. The diameter and the winding pitch were optimized because the windings in the dielectric base  $\epsilon = 3.2$  led to a decrease in their diameter.

Each of the two helical windings goes to its connector. The radiator and the LNA block with

filters are installed on a common flange and are hidden under a radiotransparent polyamide case. The radiator and assembled unit are shown in Figure 6 b-d.

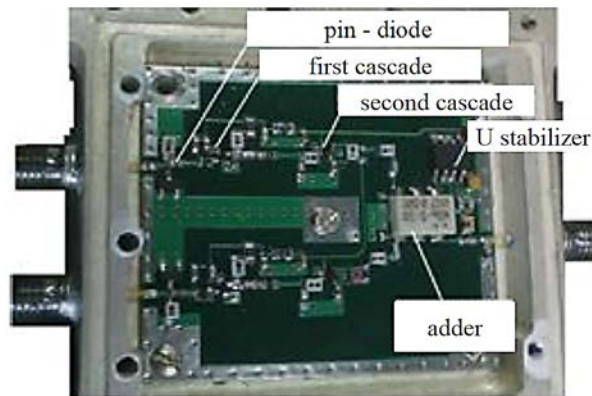


**Figure 5:** The low-noise amplifier with two outputs to a passive antenna radiator.

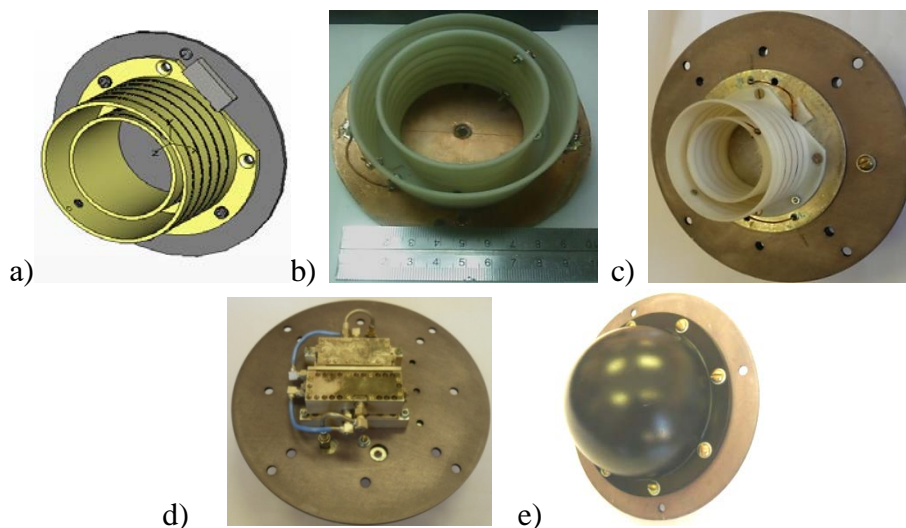


**Figure 6:** Radiator of the reflector antenna: a) 3-dimensional model; b) The model of a helix that was wound around dielectric-polyamide; c) The antenna on the base; d) Waveguide filters with the LNA e) The assembled radiator under the fairing unit.

Measured characteristics of the radiation are shown in Figures 7 and 8.

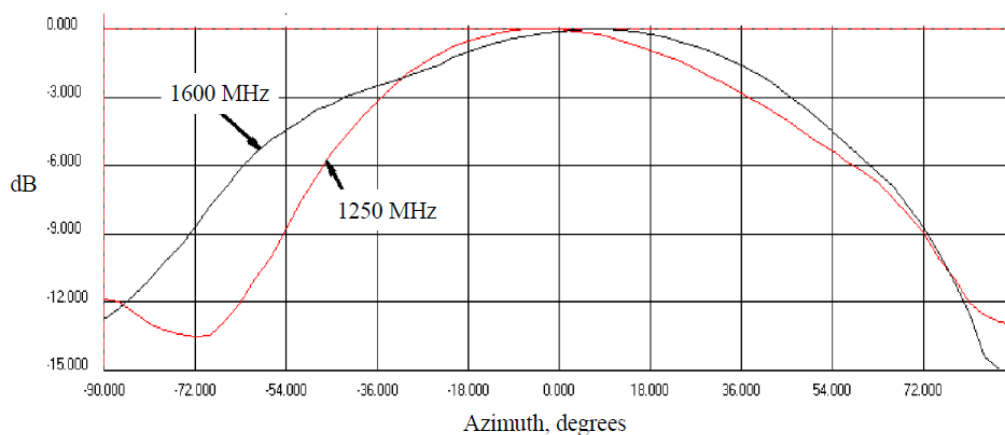


**Figure 7:** Radiation pattern sections of the radiator that were measured from the output of channel 1 (1600 MHz) at the central frequencies of the operating ranges.

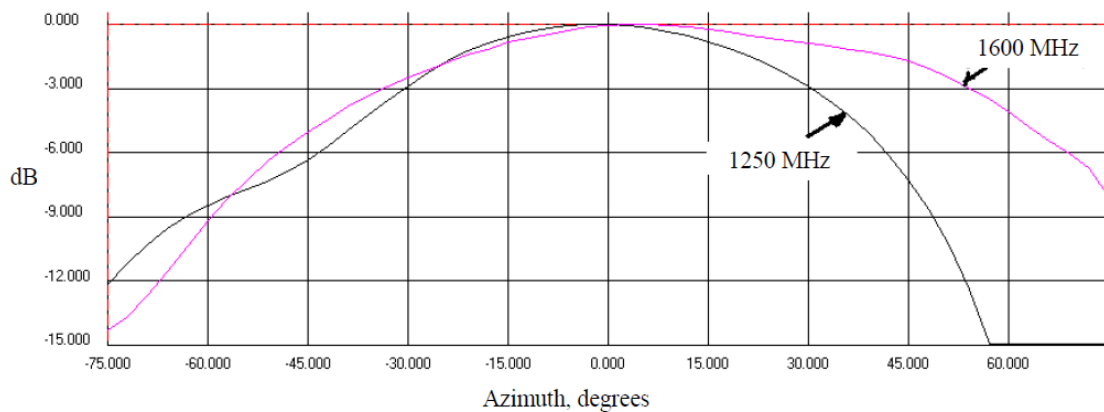


**Figure 8:** Radiation pattern sections of the radiator that were measured from the output of channel 2 (1250 MHz) at the central frequencies of the operating ranges.

### 3. CONCLUSION

We conducted the theoretical analysis on the mutual influence of helical antennas nested “into each other” on the same axis and based on the model that consists of the two rings shows that under certain conditions this interaction is low. To reduce the mutual influence, we need to use the sufficiently thin wire to make helixes for the two helical antennas. The experiment confirmed the results of calculations and modeling.

The principle to nest helical antennas “into each other” can be used when combining two or more operating frequency ranges.

### 4. AVAILABILITY OF DATA AND MATERIAL

Data can be made available by contacting the corresponding author.

### 5. REFERENCES

- [1] Lan, C. W., Chang, T. H., & Kiang, J. F. (2004, June). Helical antenna for GPS applications. *IEEE Antennas and Propagation Society Symposium, 2004*, 3: 3329-3332.
- [2] Josh Rabemanantsoa and Ala Sharaiha Small-folded, Printed Quadrifilar Helix Antenna for GPS Applications (2010) 14th International Symposium on Antenna Technology and Applied Electromagnetics [ANTEM] and the American Electromagnetics Conference [AMEREM], 4S.
- [3] Sivasankar, Thota & Mohan, V.V.Murali. (2010). Helical antenna for GPS Applications.
- [4] P. G. Elliot, E. N. Rosario, R. J. Davis Novel Quadrifilar Helix Antenna Combining GNSS, Iridium, and a UHF Communications Monopole [https://www.mitre.org/sites/default/files/pdf/12\\_3123.pdf](https://www.mitre.org/sites/default/files/pdf/12_3123.pdf)
- [5] Cheng-Wei Lan, Tze-Hsuan Chang, J.-F. Kiang Helical antenna for GPS applications Computer ScienceIEEE Antennas and Propagation Society Symposium, 2004.2004
- [6] Legkiy N.M., Unchenko I.V. Formation of the direction diagram in phased antenna array. *Rossiyskiy tekhnologicheskii zhurnal (Russian Technological Journal)*. 2019; 7(2): 29-38. (in Russ.). DOI:10.32362/2500-316X-2019-7-2-29-38
- [7] Palud, S., Colombel, F., Himdi, M., & Le Meins, C. (2011). Wideband omnidirectional and compact antenna for VHF/UHF band. *IEEE Antennas and Wireless Propagation Letters*, 10, 3-6.
- [8] Ruey-Shi Chu, Kuun M.Lee, Allen T.S. Wang. Multiband, phased-array antenna with interleaved tapered-element and waveguide radiators. Patent USA 5557291.

[9] West, James B., Elsallal, Mohamed Wajih A., Multiband phased array antenna utilizing a unit cell, Patent USA 6650291.

---



**Professor Dr. Legkiy Nikolay** is Professor at Department of Radio Engineering and Telecommunication Systems MIREA - Russian Technological University, Moscow, Russia. His research covers Radio Engineering and Automation.

---